RESEARCH ARTICLE

Improved Cartosat-1 Based DEM for Flood Inundation Modeling in the Delta Region of Mahanadi River Basin, India

Abhishek Patel[1] · Prachi Pratyasha Jena[2] · Amina Khatun[1] · Chandranath Chatterjee[1]

Abstract

An accurate flood mapping is a non-structural measure that helps to reduce damages and minimizes losses. The availability of large-scale and good quality topographic input data is of great concern for such studies. The present study involves the integration of Cartosat-1 stereo image pairs (remotely sensed) and ground truth points (surveyed) to develop digital elevation model (DEM) for the Mahanadi delta in India. The integration was performed for two cases: (i) A single Cartosat-1 image at a time and (ii) Aggregation of Cartosat-1 images one after another. Both the cases involve different numbers of ground control points (GCPs) (to be integrated with Cartosat-1 images) to study the quality and suitability of DEMs for flood inundation modeling. The best one among the DEMs prepared for each Cartosat-1 image with different number of GCPs was further used for hydrodynamic modeling. The MIKE 11 model was calibrated for 2009 and validated for 2010 using cross-sections extracted from Cartosat-1 DEMs. Further, bathymetry for the MIKE 21 model was prepared using the best Cartosat-1 DEM. MIKE FLOOD model setup was prepared to simulate flood inundation for the year 2011. The results indicate that DEMs of reasonable quality can be generated by incorporating GCPs and rational polynomial coefficients. The areal extent of simulated flood using MIKE FLOOD is in reasonable agreement with the observed counterpart.

Keywords Ground control points · Cartosat-1 DEM · Flood inundation modeling · Hydrodynamic model · MIKE flood

Introduction

Floods account for one-third of the natural disasters destroying life and property of people around the world (Adikari et al., 2010). From 1953 to 2011, about 7.208 Mha area of India was affected by floods impacting about 3.19 million people every year (Planning Commission, 2013). Heavy monsoon rainfall and improper drainage systems with low carrying capacity cause flooding of the delta regions of the country (NDMA, 2008). In recent years, reducing the flood impacts and risks in the river floodplain employing non-structural measures has gained popularity (Burrel et al., 2007; Saksena & Merwade, 2015).

Most recently, the remote sensing (RS) and geographic information system (GIS) techniques are widely used for flood inundation modeling (Khan et al., 2011; Ntajal et al., 2017; Azizian and Brocca, 2020). However, there are uncertainties associated with the technologies to derive these maps (Wang and Zheng, 2005; Merwade, 2009). Accurate topographic data are crucial input to hydrological modeling (Bourdin et al., 2012; Tan et al., 2015). Improving the quality of these low-cost, remotely sensed products can add more value in mapping flood inundation areas (Hrachowitz et al., 2013). Researchers have made many attempts to evaluate the accuracy of digital elevation models (DEMs) using LiDAR data (Bhang et al., 2007), elevation data from topographic maps (Bildirici et al., 2009; Tsanis et al., 2013), photogrammetric DEMs (Mukherjee et al., 2013), and different global DEMs (Varga and Basic, 2015). Attempts have also been made to

✉ Amina Khatun
aminakhatun9286@gmail.com

[1] Agricultural and Food Engineering Department, Indian Institute of Technology Kharagpur, Kharagpur, India

[2] Odisha University of Agriculture and Technology, Bhubaneshwar, India

improve and assess the accuracy of DEMs using synthetic stereo pair and triplet (Giribabu et al., 2013), Pleiades tri-stereo pair (Nasir et al., 2015), Cartosat-1 data (Muralikrishnan et al., 2013), and SAR for TanDEN-X DEMs (Mason et al., 2016) as typical cases. Based on the review of literature, it has been found that an elevation error of about 3–5 m (Giribabu et al., 2013; Muralikrishnan et al., 2013; Nasir et al., 2015) and accuracy of about ± 16 m (Sharma & Tiwari, 2014) for flat terrain were achieved to date.

Various researchers have worked on flood hazard and risk assessment using hydraulic models like LISFLOOD-FP (Savage et al., 2016; Toda et al., 2017), HEC-RAS (Afshari et al., 2018; Javaheri & Babbar-Sebens, 2014), FLOW-R2D (Bellos & Tsakiris, 2015), SOBEK-1D/2D (Lomulder, 2004; Tarekegn et al., 2010), ISIS-1D/TUFLOW-2D (Teng et al., 2017). Many studies incorporated the coupling of 1D and 2D models for flood modeling (Brunner, 2016; DHI, 2004; Villanueva & Wright, 2006). Among all, the MIKE FLOOD model, which is a coupled 1D (MIKE 11) and 2D (MIKE 21) model, is widely used for flood inundation modeling (Jacob et al., 2020; Mani et al., 2014; Patra et al., 2016; Patro et al., 2009; Samantaray et al., 2015; Vashist & Singh, 2021).

From the reported literature, it has been found that none of the studies so far have attempted to select the optimum number of ground control points (GCPs) to obtain a good quality representative DEM for large-scale flood inundation mapping. Recently, Jena et al. (2016) prepared DEMs using Cartosat-1 stereo pair images and surveyed GCPs. However, the study was only for two river reaches (Kushabhadra and Bhargavi) in the delta region of the Mahanadi River basin. Keeping the abovementioned points in view, the present study attempts to improve the quality of DEM prepared from Cartosat-1 stereo pair images using GCPs under different cases as compared to globally available shuttle radar topography mission (SRTM) 30 × 30 m DEMs in the entire delta region of the Mahanadi River basin. The prepared Cartosat-1 DEM is further used to set up the coupled 1D-2D MIKE FLOOD model to obtain the inundation extent in the study area.

The workflow of this paper consists of four sections, viz. introduction followed by materials and methods, results and discussion, and summarizing the conclusions.

Materials and Methods

Study Area and Dataset

The delta region of the Mahanadi River basin is selected as the study area. The Mahanadi River basin is a major inter-state (Chhattisgarh, Maharashtra, Jharkhand, and Odisha)

river basin in India (CWC, 2014; NRSC, 2014), having a geographical area of about 9063 km^2 (Fig. 1). It has a surface elevation of 10–30 m and a coastline extending for about 200 km. It has a tropical climate with an average annual rainfall of about 1500 mm.

In this study, four types of datasets are used: (i) Surveyed topographic dataset: point elevation for 4574 locations (310 elevation points in river floodplain and 4264 elevation points at 163 river cross-section profiles), (ii) Remote sensing dataset: twelve stereo pair images from IRS Cartosat-1 satellite covering the entire study area (Fig. 2) and SRTM 30 × 30 m DEM, (iii) Hydrologic dataset: discharge and water level at different gauging stations, and (iv) Archive data: historical flood data imagery for September 2011 obtained from Bhuvan, India. Tables 1–2 summarize the complete dataset's details with respect to their location, period and source.

Methodology

Cartosat-1 DEM Extraction and Quality Assessment

A DEM of reasonable quality can be produced from stereo pairs of Cartosat-1 images (Jena et al., 2016). In this study, remotely sensed data (here Cartosat-1 images) and surveyed data (GCPs) were integrated to develop good quality DEMs. The Cartosat-1 data products contain stereo photographs along with rational polynomial coefficients (RPCs). RPCs are the coefficients generated through mathematical model (rational polynomial model) which map the space coordinates (in 3D) into the image coordinates (in 2D). Technically, these are the ratio of two cubic polynomials and, hence, free from sensor parameter (Singh et al., 2008). An important aspect in DEM preparation is to generate ortho-images for subsequent analysis of the model. Ortho image is an image that shows ground objects in their true map or so-called orthographic projection. The procedure for preparing ortho-images involves the following steps: (i) Interior orientation, (ii) Exterior orientation, (iii) Tie point generation, (iv) Triangulation, (v) Model refining using GCPs, and (vi) DEM generation (Fig. 3). All the above operations were performed on the Cartosat-1 images using Photogrammetry Tool of ERDAS IMAGINE 2015. The DEMs were prepared under two cases: (i) DEM from single image stereo-pair at a time, and (ii) DEM from aggregated image pairs one after the other. Zero, four, eight, twelve and 'All GCPs' were considered in the refinement process of Cartosat-1 DEM for the former case, whereas only zero and 'All GCPs' were considered for the latter (Fig. 4). A total of 240 GCPs were used to generate DEMs of 10 × 10 m spatial resolution. The prepared Cartosat-1 DEMs (10 × 10 m) and freely available SRTM DEM (30 × 30 m) were then evaluated against
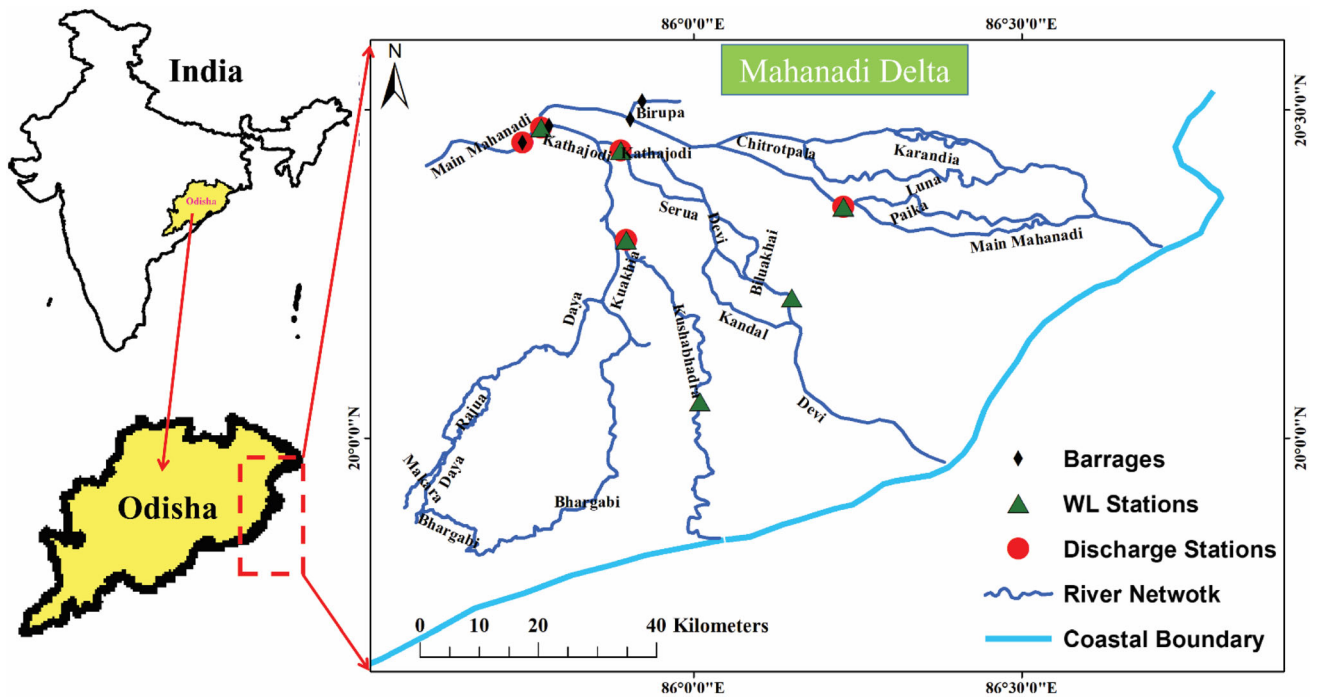
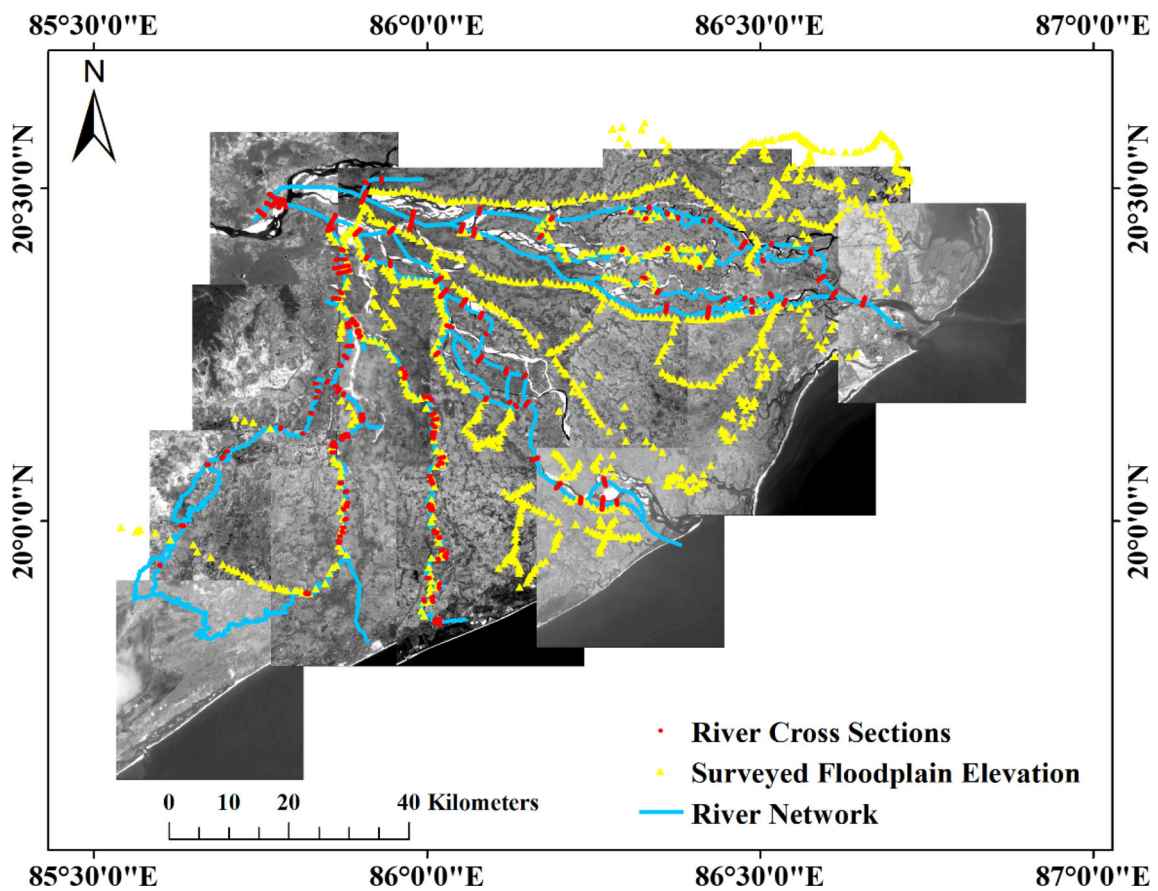**Fig. 1** Location map of the delta region of the Mahanadi River basin

Fig. 2 Cartosat-1 images with surveyed floodplain elevation and surveyed river cross-section points

Table 1 Details of Cartosat-1 images used in this study

Sl. no.	Image (part-row)	Image ID	Date of pass	Source
1	580–302	b2	January 10, 2011	NRSC Hyderabad, India
2	580–303	b3	December 26, 2008	
3	581–302	c2	December 30, 2010	
4	581–303	c3	December 30, 2010	
5	582–302	d2	March 20, 2010	
6	582–303	d3	March 20, 2010	
7	580–304	b4	March 20, 2010	
8	581–304	c4	December 30, 2010	
9	582–304	d4	March 20, 2010	
10	583–302	e2	April 13, 2011	
11	583–303	e3	April 13, 2011	
12	584–302	f2	December 10, 2011	

Table 2 Details of water level, discharge and surveyed elevation dataset

Type of data	Location	Period	Source
Water level	Naraj	2009, 2010, 2011	CWC, Bhubaneswar
	Cuttack, Tarapur, Balianta	2009, 2010, 2011	SSWDC, Bhubaneswar
Discharge	Cuttack, Tarapur, Naraj, Balianta	2009, 2010, 2011	SSWDC, Bhubaneswar
Surveyed river cross-sections	Different rivers in delta region	–	Superintendent cop. of India
Surveyed flood-plain elevation	Floodplain area of delta region	–	Superintendent cop. of India
SRTM DEM (30 × 30 m)			USGS Earth Explorer

surveyed elevation for floodplain points and river cross-section profiles (Fig. 5) using standard deviation (SD) and root-mean-square error (RMSE).

Hydrodynamic Flood Modeling

The coupled 1D-2D MIKE FLOOD model was used for flood inundation modeling (Chatterjee et al., 2008). Details of this coupling can be found in the literature (Patro et al., 2009; Samantaray et al., 2015). The MIKE 11 model was set up with five core setup files: river network file, river cross-sections file, boundary conditions file, hd parameter file, and simulation file. For such a large area (9063 km^2) of the Mahanadi delta, consideration of all the major and minor rivers with their finer distributaries create a complex network system which would further complicate the model setup and the simulation of floods. So, to keep the model setup simpler and to enable faster flood simulations, the finer distributaries of river network were excluded in formulating the model setup in the river network file. The MIKE 11 model was calibrated and validated for the 4 months of southwest monsoon season (July–October) of 2009 and 2010, respectively, using discharge and water-level data. Since the delta region of the Mahanadi River basin is highly flood-prone during the monsoon season,

flood inundation mapping was carried out for the four monsoon months only. Further, for performance evaluation of MIKE 11, five different statistical criteria namely root-mean-square error (RMSE), coefficient of determination(R^2), nash–sutcliffe efficiency (NSE), index of agreement (d), and percentage deviation in peak (% Dev.) were used. The MIKE 21 is a 2D model which simulates the surface flow and its extent over floodplain connected to river source in flooding condition (DHI, 2014). This model was set up with the bathymetry (MIKE format for DEM) and Manning's roughness coefficient (n) data. The Cartosat-1 DEM was resampled in ArcGIS 10.1 software to generate the bathymetry file of 250 × 250 m spatial resolution.

The MIKE 11 and MIKE 21 models were coupled in the MIKE FLOOD module (Fig. 5) to simulate the flood inundation for the year 2011. As the current study is intended to simulate the flood condition (discharge and water level overtopping the banks of rivers), model simulation was performed only for the peak discharge period of 2011. The peak flow period was identified from observed flood inundation data, and hence, the simulation in the MIKE FLOOD model was carried out from September 4 to 24 for the year 2011. To keep the model stable with desired time-step and allowable Courant Number, and straight

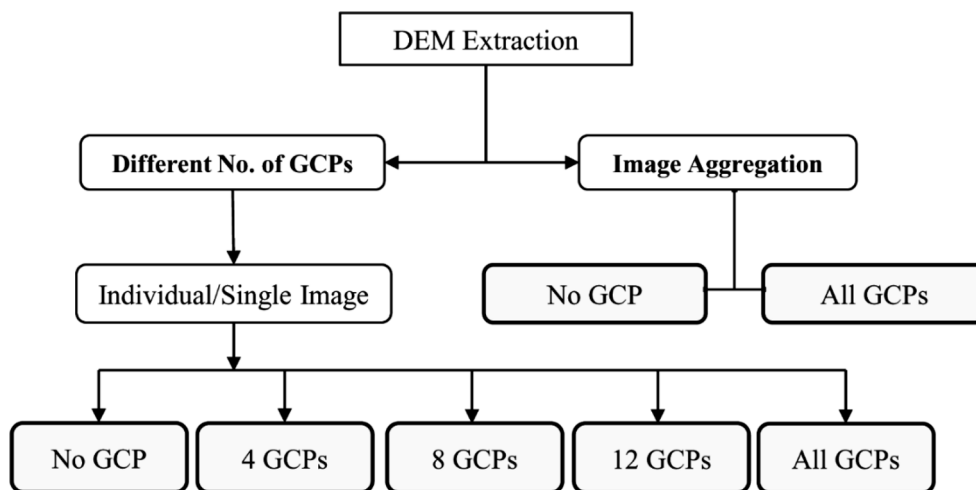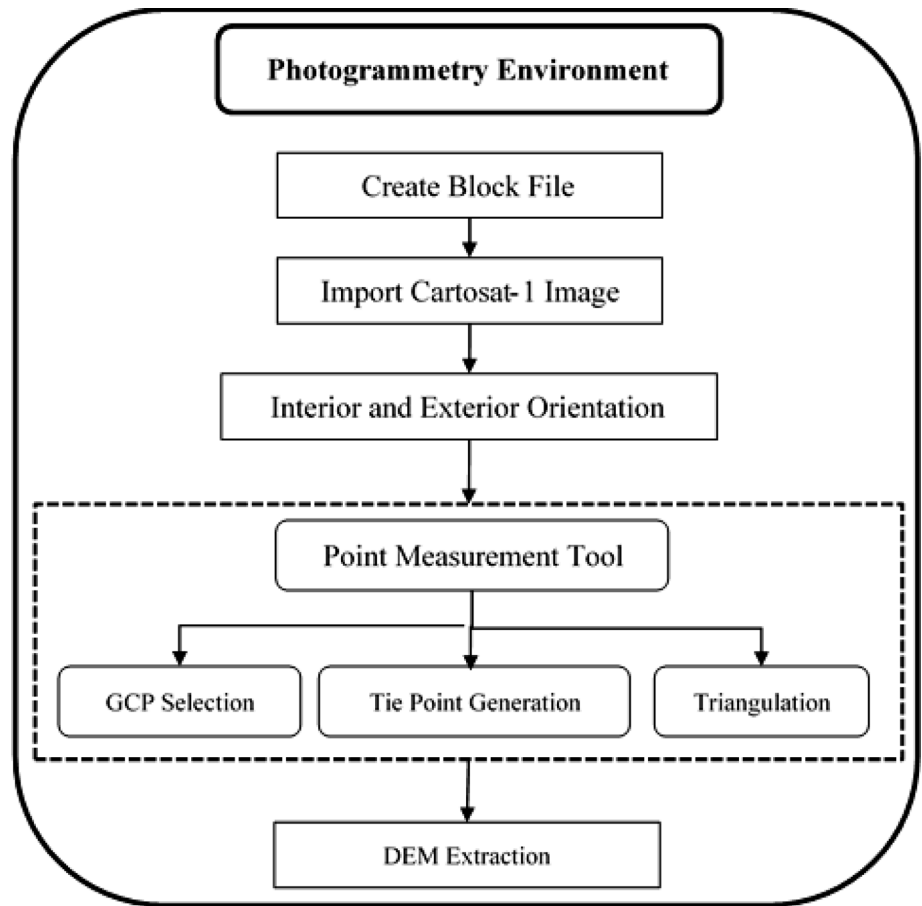Fig. 3 Flowchart showing the
process of DEM generation

Fig. 4 Representation of different cases and sub-cases for Cartosat-1 DEM generation

forward with faster simulations for such a large area (9063 km^2), the MIKE 21 single grid (SG) module was used in this study. This simulated flood extent was compared with the observed flood inundation maps (https://bhuvan-app1.nrsc.gov.in/disaster/disaster.php) for the same year using a measure of fit 'F' (Eq. 1). The measure of fit (F) is defined as the ratio of areas of overlapped observed and simulated inundation extent (IE) to that of both overlapped and un-overlapped observed and simulated inundation extent (Bates & De Roo, 2000). A higher value of F indicates better matching of the flood inundation extent simulated by MIKE FLOOD with the observed one.
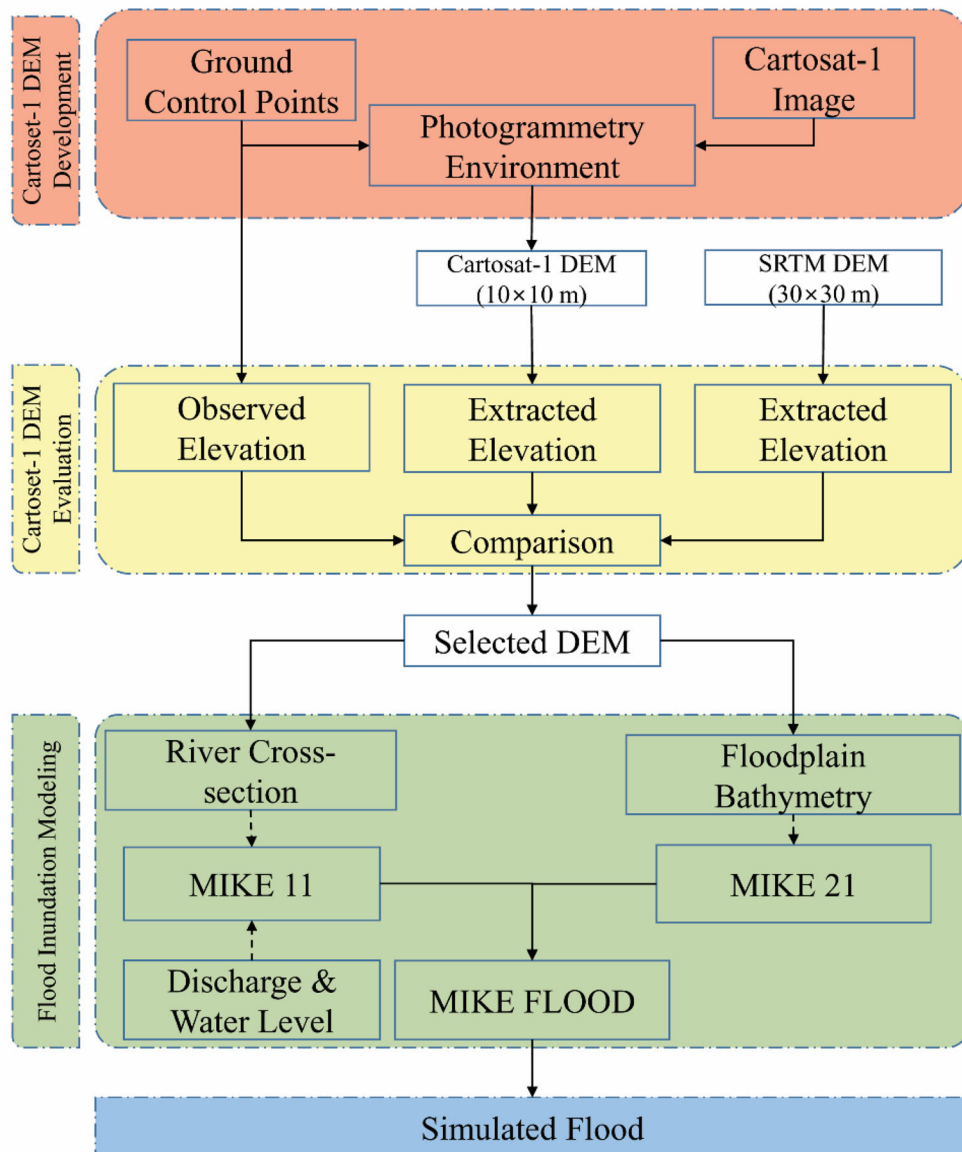
Fig. 5 Illustration of methodology adopted for Cartosat-1 DEM extraction, evaluation and flood inundation modeling

$$F = \left[\frac{IE_{obs} \cap IE_{mod}}{IE_{obs} \cup IE_{mod}} \times 100 \right] \qquad (1)$$

where IE_{obs} and IE_{mod} are the inundation extents for observed and simulated floods.

Results and Discussion

Cartosat-1 DEM from Multiple Images in Aggregation

The quality of Cartosat-1 DEMs generated with image aggregation is described in this section. The SDs for the

DEMs generated using rational polynomial coefficients (RPCs) only are found to be in the range of 3.36–62.06 m, while the RMSE for the same ranged from 4.33 to 64.77 m. Interestingly, the values of SD and RMSE are found to be in the range of 3.3–67.25 and 4.29–6.31 m, respectively, for DEMs generated using RPCs along with GCPs. The graphical representation of these statistics for both types of Cartosat-1 DEMs generated using different numbers of GCPs is presented in Fig. 6. From Fig. 6, it is observed that in the case of aggregation of Cartosat-1 images, the error measures (both SD and RMSE) get added up and reach a value of about 60–70 m with an RPCs-only scenario. In contrast, the DEMs generated with both RPCs and GCPs exhibit an error (both SD and RMSE) limited to a value of
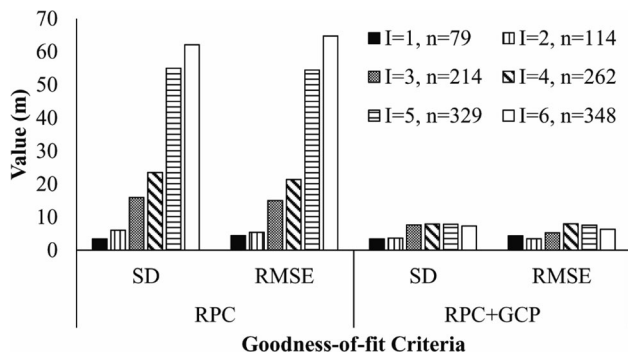
Fig. 6 SD (m) and RMSE (m) for Cartosat-1 DEM for image aggregation cases (i) only RPC, and (ii) RPC with GCPs

10 m. From this result, it can be inferred that the incorporation of surveyed GCPs improves the quality of the DEMs produced.

Cartosat-1 DEMs from Individual Images

In this case, a total of sixty different Cartosat-1 DEMs were prepared, taking a single image out of twelve images at a time with five sub-cases for each (no-, four-, eight-, twelve- and All-GCPs) (Fig. 4). Firstly, the quality of all the individual DEMs prepared was evaluated against surveyed elevation points in the floodplain (Table 3). It is observed from Table 3 that the RMSE for DEMs prepared with RPCs-only is relatively high (RMSE = 4.87–134.84 m). However, in DEMs prepared with RPCs and 'All GCPs', the RMSE ranges only from 1.30 to 13.31 m which indicates that GCPs show better results than RPCs-only scenario for all the cases. In case of $b3$, $b4$ and $c4$, the higher RMSE values for both RPCs and GCPs scenarios can be attributed to the fact that the surveyed GCPs are concentrated in some portions of the image, i.e., the GCPs are not evenly distributed. It is also observed for some cases, like $b3$, $c3$ and $c4$, that the RMSE increased when more than

four GCPs were added. For these images, points from Google Earth were taken as GCPs due to lack of survey points on these images. Since the Google Earth-derived points are less accurate than surveyed GCPs, higher RMSE is observed in these images. This shows that the horizontal (latitude and longitude) and vertical (altitude) accuracy of GCPs is the key factor for a good-quality DEM generation. Then, based on the error criteria, the best of each sub-case's DEM was selected and mosaicked. Elevations for 333 floodplain points (which were not used for DEM generation) were extracted from the Cartosat-1 DEM and compared with surveyed values (Fig. 7a). It is observed that most of the points adhere to the 1:1 line indicating that the elevations extracted from the Cartosat-1 DEM are nearly the same as that of the surveyed elevations of the floodplain. Finally, the quality assessment of prepared DEMs was done for river cross-section suitability. River cross-section profile values corresponding to surveyed locations are extracted from the DEMs (Cartosat-1 DEMs and SRTM DEMs) and compared (Fig. 8). This comparison indicates that extracted cross-sections from Cartosat-1 DEMs follow a very similar profile as observed, which is not valid in cases of the SRTM DEM. Also, the scatter plot between observed and extracted (from mosaicked Cartosat-1 DEMs) elevations points from river cross-sections exhibit good agreement. A total of 2476 points from different cross-sections were considered in this case (Fig. 7b). Hence, this assessment (for floodplain and river cross-sections) indicates better accuracy of Cartosat-1 DEMs for topographic data and relatively higher suitability for hydrodynamic modeling over the freely available global SRTM DEMs.

Table 3 RMSE (m) of individual Cartosat-1 DEMs

Image	Only RPCs	04 GCPs	08 GCPs	12 GCPs	All GCPs (no. of GCPs)	SRTM
$b2$	6.23	5.03	3.74	3.37	2.93 (22)	3.60
$c2$	4.87	2.24	1.93	1.84	1.71 (18)	3.52
$d2$	5.83	1.50	1.39	1.36	1.31 (23)	3.15
$e2$	134.84	4.07	2.56	4.14	2.12 (21)	4.96
$f2$	39.25	2.01	1.59	1.22	1.45 (14)	1.94
$b3$	8.03	3.80	10.34	12.62	6.82 (18)	2.85
$c3$	6.30	3.19	4.92	6.81	2.72 (26)	3.20
$d3$	10.34	2.47	2.93	2.86	2.68 (27)	3.07
$e3$	10.14	1.54	2.21	1.53	1.30 (18)	1.85
$b4$	28.72	22.74	14.11	13.31	13.31 (12)	3.56
$c4$	37.22	1.69	10.89	9.42	5.68 (18)	2.83
$d4$	102.89	2.37	4.90	2.35	1.70 (23)	2.03
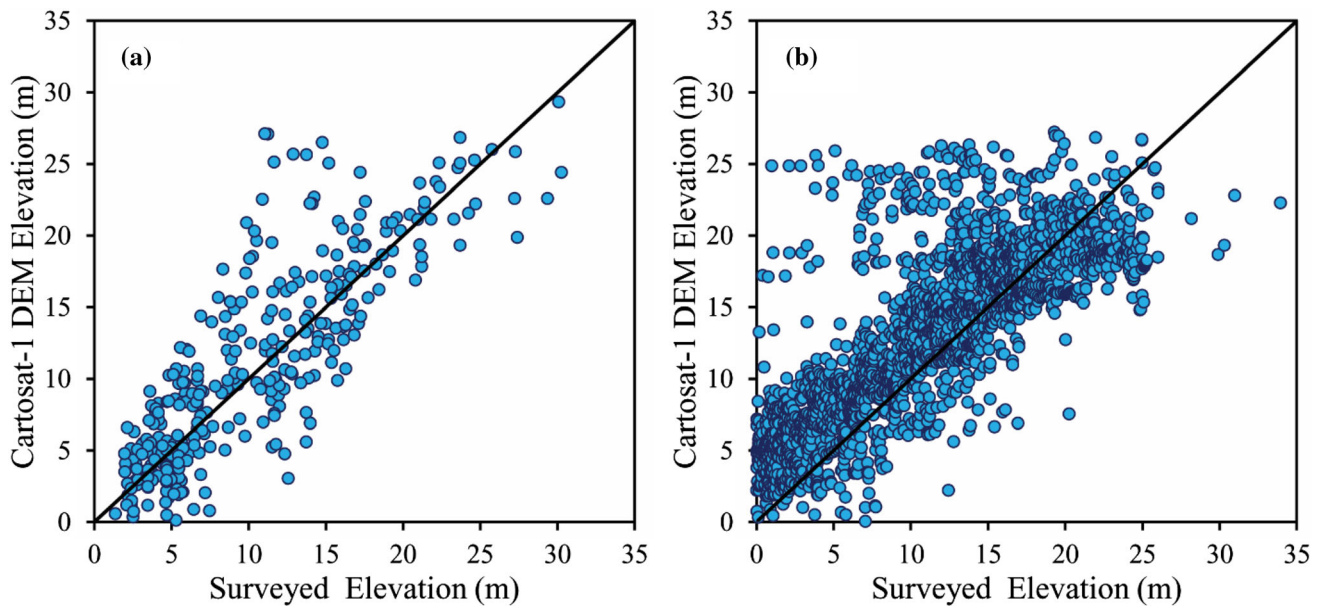
Fig. 7 Comparison of Cartosat-1 DEM derived elevations and surveyed elevations **a** in floodplain, and **b** at river cross-sections
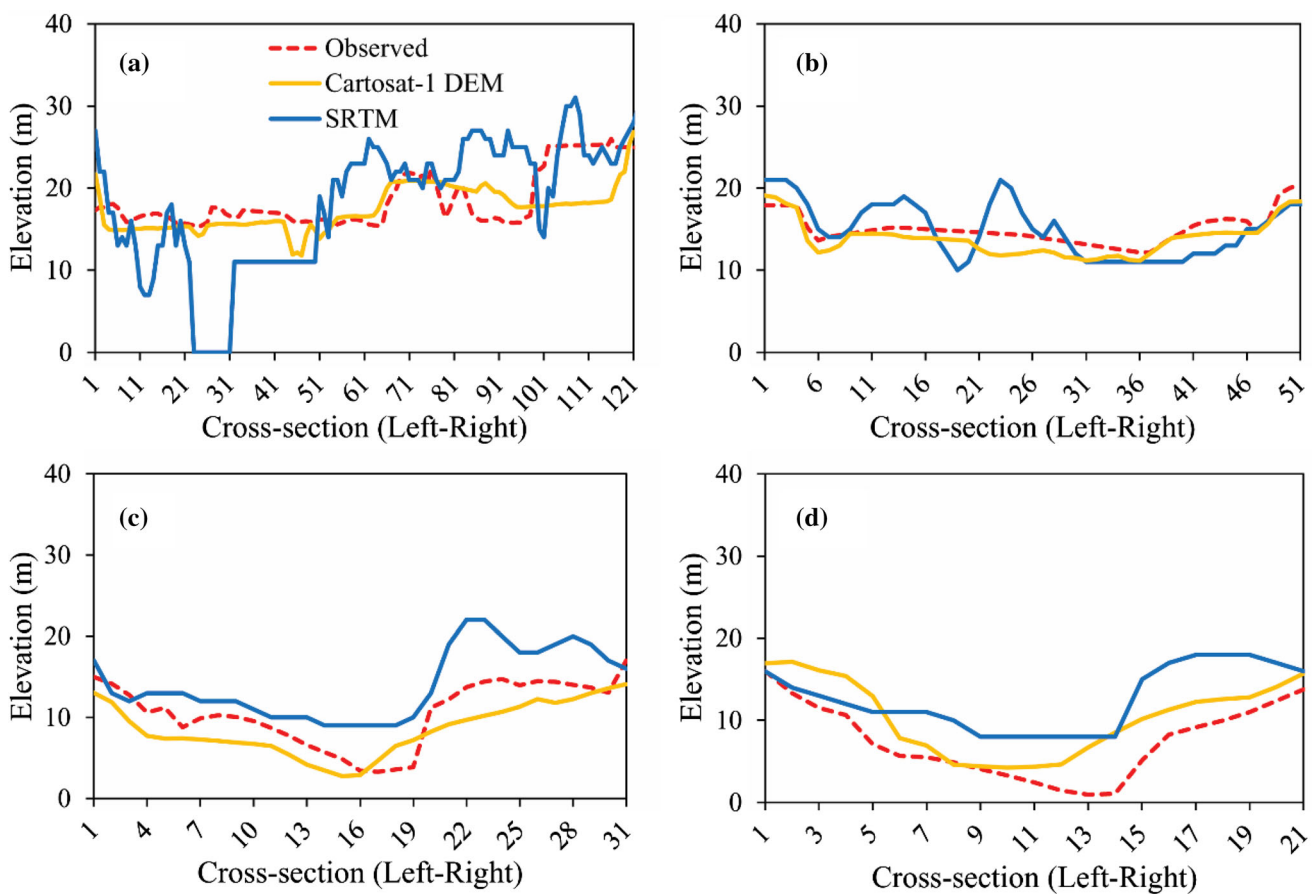
Fig. 8 River cross-section profiles for different sections on images **a** *b*2, **b** *c*2, **c** *b*3, and **d** *c*3

Table 4 Error measures for discharge and water level at different gauging stations during calibration (2009)

Error measure	Name of discharge (D) & water level (WL) gauging station							
	Naraj		Tarapur		Cuttack		Balianta	
	D	WL	D	WL	D	WL	D	WL
RMSE, m³/s	2834.5	0.96	391.7	0.83	583.12	0.96	168.81	0.73
R^2	0.71	0.95	0.8	0.88	0.78	0.92	0.92	0.92
NSE	0.82	0.41	0.80	0.53	0.89	0.73	0.83	0.68
Index of agreement (d)	0.94	0.9	0.95	0.89	0.97	0.9	0.96	0.92
Percentage deviation in peak, %	−31.68	−0.74	−6.48	7.21	−16.35	−7.24	−4.19	1.01
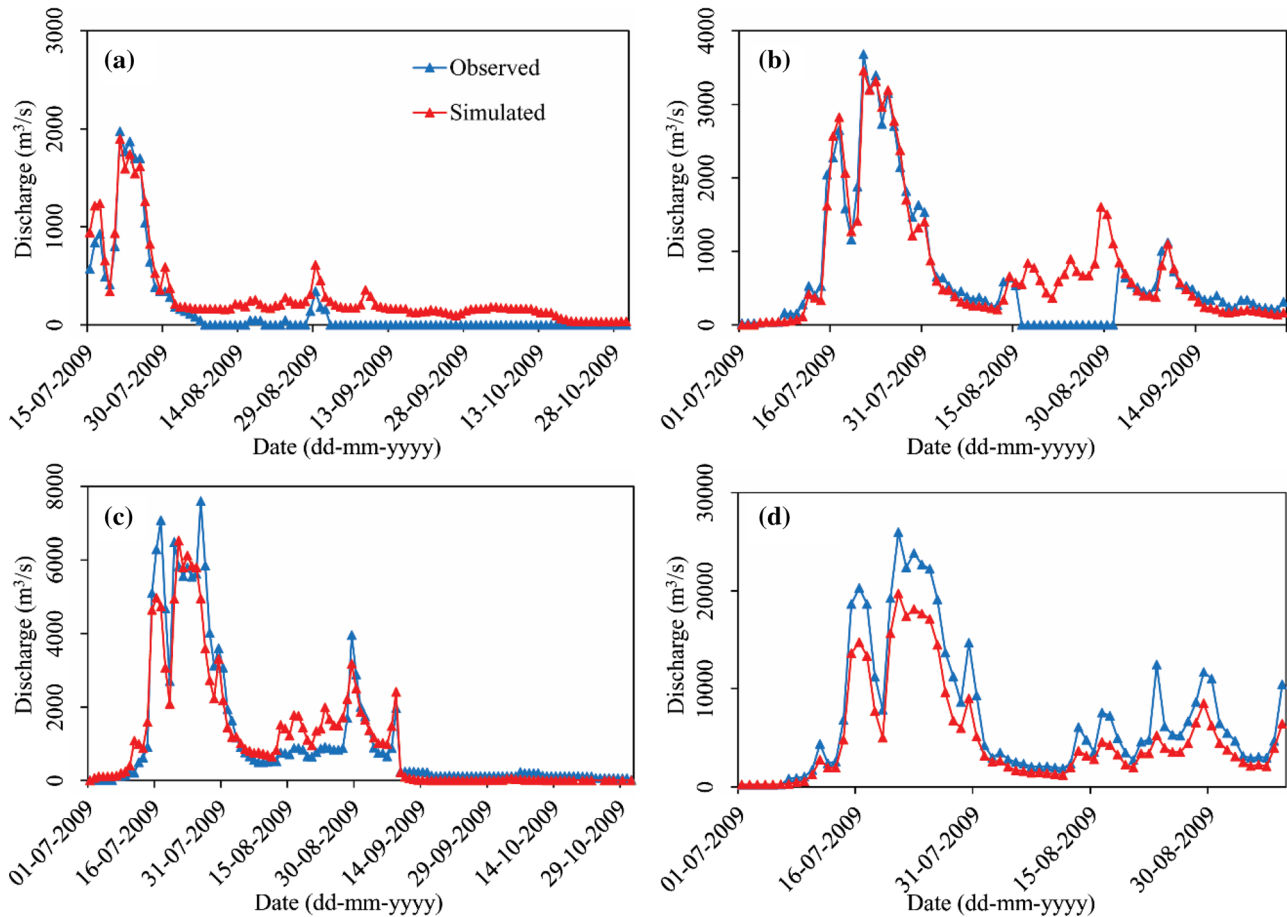
Fig. 9 Comparison of observed and simulated discharges at **a** Balianta, **b** Tarapur, **c** Cuttack, and **d** Naraj during calibration (2009)

Flood Inundation Modeling

Calibration and Validation of MIKE 11 HD Model

The MIKE 11 HD model was calibrated for the monsoon season of the year 2009 using water level and discharge data. From Table 4, it can be seen that the RMSE for Naraj is very high, i.e., 2835.5 m³/s. This may be because the storage structures at Naraj, Kathajodi and Birupa were not incorporated in the model. The index of agreement

(d) values varies in the range 0.94–0.97 and 0.89–0.92 for discharge and water level, respectively. This model is also found to simulate the peak discharge and water levels relatively well. Overall, the evaluation of the MIKE 11 HD model based on the five goodness-of-fit criteria, as shown in Table 4, indicates satisfactory performance during the calibration process. Also, Figs. 9–10 confirm that the simulated discharges and water levels are in reasonable agreement with their observed counterparts. Since the water stored and diverted flow, in actual condition, were
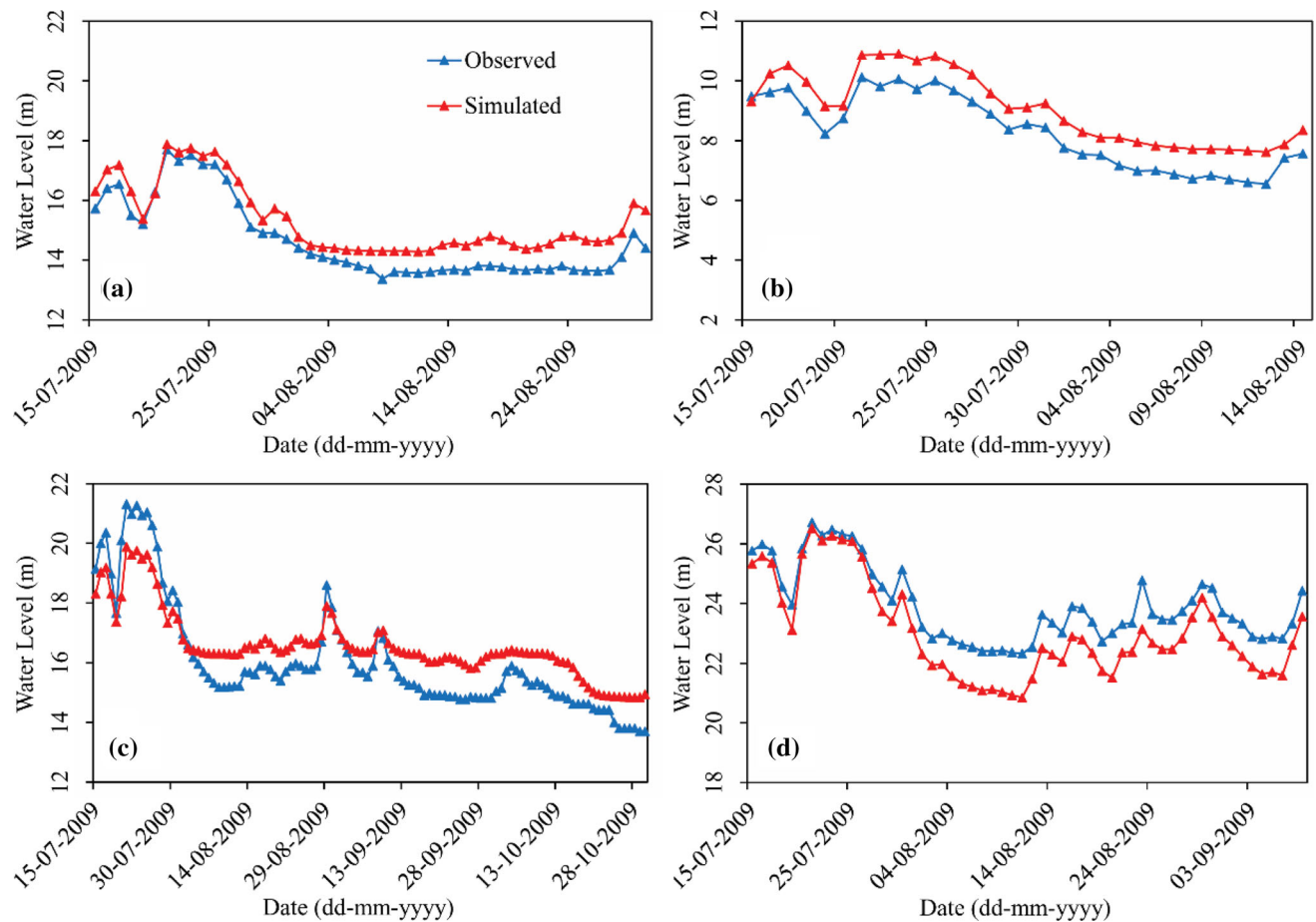
Fig. 10 Comparison of observed and simulated water levels at **a** Balianta, **b** Tarapur, **c** Cuttack, and **d** Naraj during calibration (2009)

Table 5 Error measures for discharge and water level at different gauging stations during validation (2010)

Error measure	Name of discharge (D) & water level (WL) gauging station			
	Naraj		Tarapur	
	D	WL	D	WL
RMSE, m^3/s	1300.34	0.67	201.54	0.6
R^2	0.81	0.96	0.84	0.9
NSE	0.92	0.63	0.87	0.48
Index of agreement (d)	0.98	0.93	0.98	0.87
Percentage deviation in peak, %	−19.28	−0.34	10.69	0.82

added to the modeled flow, the simulated discharges are more than the observed ones (Samantaray et al., 2015).

After calibration of the MIKE 11 HD model, it is validated for the monsoon season of the year 2010. Performance evaluation of the MIKE 11 HD model during validation is presented in Table 5 and Fig. 11. From Table 5 and Fig. 11, it is evident that the MIKE 11 HD model performed satisfactorily during validation. Further, this model setup is coupled with MIKE 21 model for

simulating the flood inundation using the MIKE FLOOD model.

Flood Inundation Simulation and Validation

Finally, the MIKE FLOOD was set up by coupling MIKE 11 and MIKE 21 models to simulate flood inundation (extent and depth) for the peak discharge period (September 4–24, 2011). The results obtained from MIKE FLOOD (Fig. 12a) shows that the maximum extent of flood covers
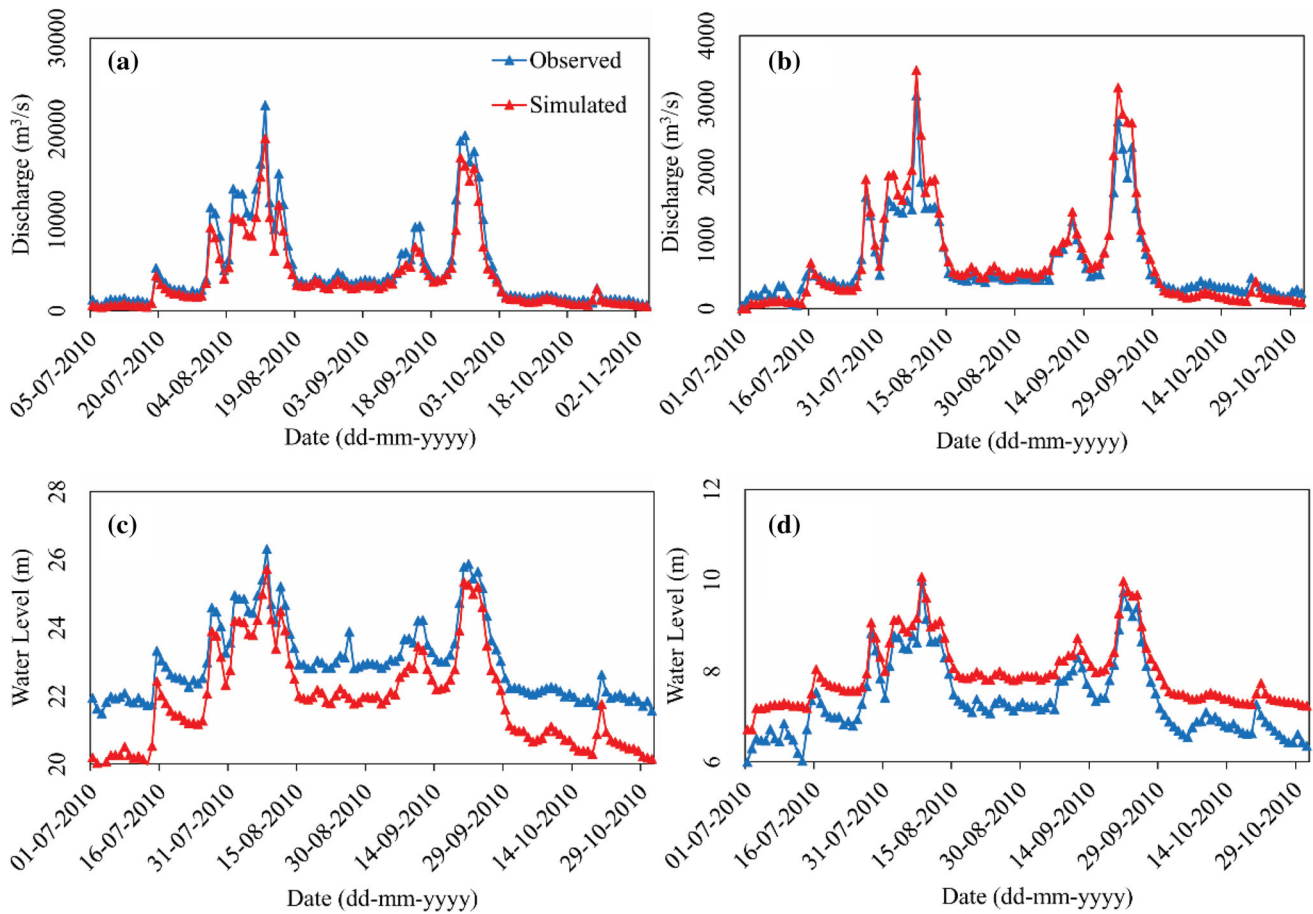
Fig. 11 Comparison of observed and simulated discharges and water levels at **a** Naraj, and **b** Tarapur during validation (2010)
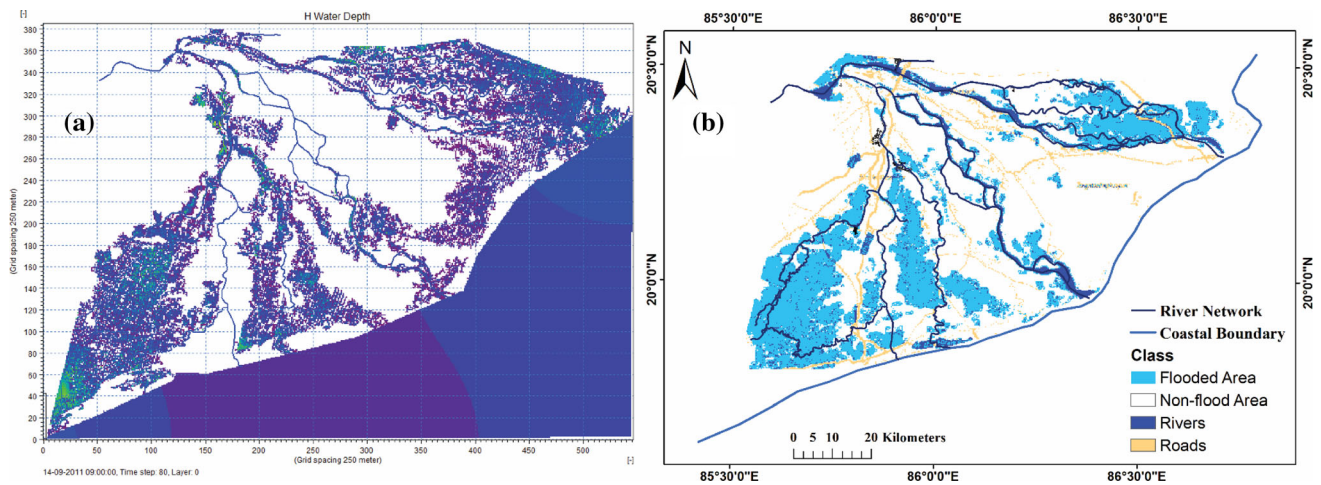
Fig. 12 Flood inundated area obtained from **a** MIKE FLOOD simulation, and **b** observed flood data archive of Bhuvan, India

an area of about 2399.31 km^2. Out of the total flooded area, about 1734.56 km^2 and 664.75 km^2 areas were found to have flood depth of 0–4 m and more than 4 m, respectively. Historical flood data imagery taken from Bhuvan,

India, for flood date September 14, 2011, was used to validate the MIKE FLOOD simulation (Fig. 12b). The areas under different fit parameters described in Eq. 1 are shown in Table 6. Table 6 indicates that the modeled flood

Table 6 Fit measure for evaluating the performance of MIKE FLOOD model for September 14, 2011

Parameters for fit measure	Area under fit parameter (km^2)	Fit measure (%)
IE_{obs}	1825.4375	35.74
IE_{mod}	2399.3130	
$IE_{obs} \cap IE_{mod}$	1112.1875	
$IE_{obs} \cup IE_{mod}$	3112.5630	
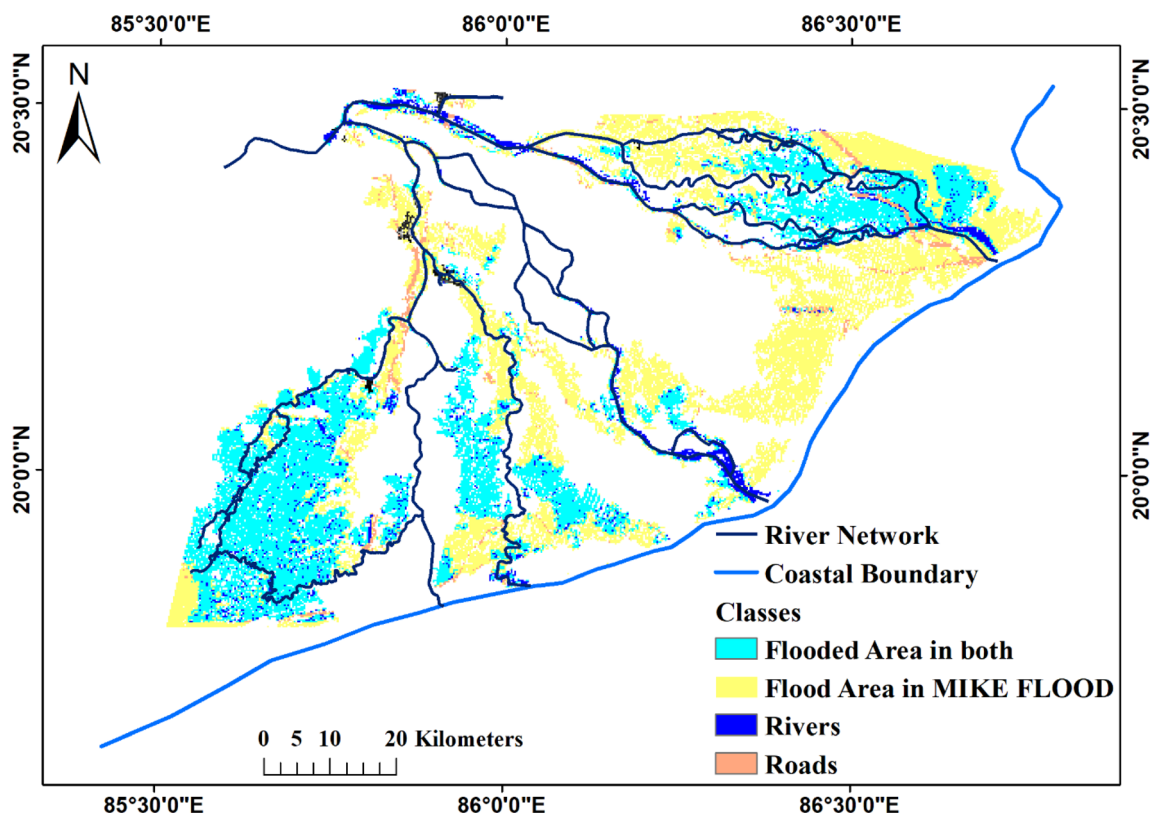
Fig. 13 Comparison of flood inundation extent for September 2011 obtained from MIKE FLOOD model and historical flood data of Bhuvan, India

extent (2399.31 km^2) is more than the observed (1825.4375 km^2) one. It is also found that the developed MIKE FLOOD model can simulate 35.74% of the inundated area accurately for the year 2011. Comparison of simulated and observed flood inundations (Fig. 13) indicates that the areal mismatch of flood extent is obtained at locations close to the Bay of Bengal. This mismatch may be due to the exclusion of finer river distributaries at shallow terrain of the delta near the Bay of Bengal during model development. It may be noted that, as this study focuses on the fluvial or riverine flooding due to high river discharge from the upper reaches of the Mahanadi basin during the monsoon season (June–September), the downstream boundary was considered as low water level (sea level) boundary condition. This could also be a possible reason for the areal mismatch of flood inundation for the particular flooding event. Moreover, the low fit of the

flooded area may collectively be attributed to the absence of structures (barrages) on main rivers, escapes, and canals and their related operations in the model setup due to data limitation. However, the simulated flood inundation pattern is similar to that of observed. Overall, based on the findings of Wilson et al. (2007) and Samantaray et al. (2015), the flood inundation simulated by the developed MIKE FLOOD model can be considered satisfactory for data-scarce conditions.

Summary and Conclusions

The quality of outputs from flood inundation modeling, in terms of both space (areal extent) and time (duration of ponding), is dependent on the quantity and quality of input data provided to the hydrodynamic model. The present

study tried to improve the quality of DEMs used for flood inundation studies in hydrodynamic modeling by integrating accurately surveyed GCPs with Cartosat-1 data. It compared the quality of DEMs prepared with and without GCPs and the globally available SRTM 30 × 30 m DEM. Further, the prepared Cartosat-1 DEM is used to set up the hydrodynamic models; MIKE 11 and MIKE 21; finally, these two modules are coupled in the MIKE FLOOD model. The study concludes that the errors accumulate if the Cartosat-1 images are aggregated with RPCs only for DEM generation. In contrast, GCPs added along with RPCs give better quality DEM with image aggregation. On the other hand, the Cartosat-1 DEMs prepared using a single image with RPCs only and RPCs along with GCPs reveal the importance of GCPs in photogrammetry to prepare good-quality Cartosat-1 DEMs to obtain floodplain elevation and cross-section profiles for flood inundation modeling. The results also indicate that the cross-sections derived from Cartosat-1 DEMs are better representative of the observed river cross-sections than SRTM DEM. However, the quality of the prepared DEMs can be further improved with GCPs well spread all over the area covered in a Cartosat-1 image. The locations of the GCPs should therefore be skillfully selected to obtain a better representative DEM. The inundation extent and pattern simulated by the MIKE FLOOD model are found to be showing satisfactory agreement with the flood archive of remotely sensed data. Low fit measure obtained for model performance assessment justifies neglecting the channel breaching and limited representation of channel network in the entire study area, which causes spatial inconsistency in flood inundation mapping by the model.

Declarations

References

Adikari, Y., Osti, R., & Noro, T. (2010). Flood-related disaster vulnerability: An impending crisis of megacities in Asia. *Journal of Flood Risk Management, 3*, 185–191. https://doi.org/10.1111/j.1753-318X.2010.01068.x

Afshari, S., Tavakoly, A. A., Rajib, M. A., Zheng, X., Follum, M. L., Omranian, E., & Fekete, B. M. (2018). Comparison of new generation low-complexity flood inundation mapping tools with a hydrodynamic model. *Journal of Hydrology, 556*, 539–556. https://doi.org/10.1016/j.jhydrol.2017.11.036

Azizian, A., & Brocca, L. (2020). Determining the best remotely sensed DEM for flood inundation mapping in data sparse regions. *International Journal of Remote Sensing, 41*(5), 1884–1906. https://doi.org/10.1080/01431161.2019.1677968

Bates, P. D., & De Roo, A. P. J. (2000). A simple raster-based model for flood inundation simulation. *Journal of Hydrology, 236*(1), 54–77. https://doi.org/10.1016/S0022-1694(00)00278-X

Bellos, V., & Tsakiris, G. (2015). Comparing various methods of building representation for 2D flood modelling in built-up areas. *Water Resources Management International Journal Published for the European Water Resources Association (EWRA), 29*(2), 379–397.

Bhang, K. J., Schwartz, F. W., & Braun, A. (2007). Verification of the vertical error in C-band SRTM DEM using ICESat and Landsat-7, Otter Tail County, MN. *IEEE Transactions on Geoscience and Remote Sensing, 45*(1), 36–44. https://doi.org/10.1109/TGRS.2006.885401

Bildirici, O. I., Ustun, A., Selvi, Z. H., Abbak, A. R., & Bugdayci, I. (2009). Assessment of shuttle radar topography mission elevation data based on topographic maps in Turkey. *Cartography and Geographic Information Science, 36*(1), 95–104. https://doi.org/10.1559/152304009787340205

Bourdin, D. R., Fleming, S. W., & Stull, R. B. (2012). Streamflow modelling: A primer on applications approaches and challenges. *Atmosphere-Ocean, 50*(4), 507–536. https://doi.org/10.1080/07055900.2012.734276

Brunner, G. W. (2016). HEC-RAS river analysis system-user's manual version 5.0. US army corps of engineers. Institute for water resources, hydrologic engineering center (HEC), p. 962.

Burrel, B. C., Davar, K., & Hughes, R. (2007). A review of flood management considering the impacts of climate change. *Water International, 32*(3), 342–359. https://doi.org/10.1080/02508060708692215

Chatterjee, C., Förster, S., & Bronstert, A. (2008). Comparison of hydrodynamic models of different complexities to model floods with emergency storage areas. *Hydrological Processes, 22*(24), 4695–4709. https://doi.org/10.1002/hyp.7079

CWC (2014). Central water commission, ministry of water resources, New Delhi.

DHI (2004). MIKE 11: A modeling system for rivers and channels–reference manual. Danish hydraulic institute: Horsholm, Denmark.

DHI (2014). MIKE 21–2D modelling of coast and sea. DHI water & environment Pty Ltd.

Giribabu, D., Kumar, P., Mathew, J., Sharma, K. P., & Murthy, Y. V. N. K. (2013). DEM generation using Cartosat-1 stereo data: Issues and complexities in Himalayan terrain. *European Journal of Remote Sensing, 46*(1), 431–443. https://doi.org/10.5721/EuJRS20134625

Hrachowitz, M., Savenije, H. H. G., Blöschl, G., McDonnell, J. J., Sivapalan, M., Pomeroy, J. W., Arheimer, B., Blume, T., Clark, M. P., & Ehret, U. (2013). A decade of predictions in ungauged basins (PUB)—a review. *Hydrological Sciences Journal, 58*(6), 1198–1255. https://doi.org/10.1080/02626667.2013.803183

floodplains of North Carolina. *Natural Hazards Review, 6*(1), 34–40. https://doi.org/10.1061/(ASCE)1527-6988(2005)6:1(34)

Wilson, M., Bates, P., Alsdorf, D., Forsberg, B., Horritt, M., Melack, J., Frappart, F., & Famiglietti, J. (2007). Modeling large-scale inundation of Amazonian seasonally flooded wetlands. *Geophysical Research Letters, 34*(15), L15404. https://doi.org/10.1029/2007GL030156